

# A Methodology and Associated CAD Tools for Support of Concurrent Design of MEMS

B. F. Romanowicz<sup>1</sup>, M. H. Zaman<sup>1</sup>, S. F. Bart<sup>1</sup>, V. L. Rabinovich<sup>1</sup>, I. Tchertkov<sup>1</sup>, S. Zhang<sup>1</sup>  
M. G. da Silva<sup>1</sup>, M. Deshpande<sup>1</sup>, K. Greiner<sup>1</sup>, J. R. Gilbert<sup>1</sup>, Shawn Cunningham<sup>2</sup>

**Abstract:** Development of micro-electro-mechanical systems (MEMS) products is currently hampered by the need for design aids, which can assist in integration of all domains of the design. The cross-disciplinary character of microsystems requires a top-down approach to system design which, in turn, requires designers from many areas to work together in order to understand the effects of one sub-system on another. This paper describes current research on a methodology and tool-set which directly support such an integrated design process.

**keyword:** Micro-system, MEMS, CAD, macro-model, simulation

## 1 Introduction

Considerable progress in technologies for microsystems fabrication has made over the past two decades, resulting in a large variety of commercially successful devices. These products have benefited from the high performance and low manufacturing costs characteristic of MEMS batch fabrication technologies. Though the manufacturing technologies are derived from microelectronic fabrication techniques, most devices require application specific fabrication steps, which must be developed, and characterized. This often results in costly and time consuming prototyping. It is recognized that standardization of processes will help reduce the entry cost of microsystems.

MEMS sensors and actuators can be viewed as the electronic interface to the physical world. Some physical quantity of interest is transformed into an electrical quantity that can be measured, or some electrical signal is converted into some action on the environment. As a result of the small dimensions of these transducers, and the semiconductor materials often used, strong field coupling is present, and needs to be taken into account in the modeling of these devices, to accurately capture their behavior. Historically, most of the modeling and simulation effort has gone into developing tools that capture the intricate physics present in MEMS devices.

All MEMS systems have some common layers to their design. These include device design (design a manufacturable component), package design (design a practical package), and system

design (design and improve the system the device fits into). The requirement for design aids is best illustrated by considering the MEMS products that have been commercially successful to date. Examples include inkjet printer nozzles, pressure sensors, and a variety of inertial sensors used primarily in the automotive field. In all of these products, the design criteria for each of the individual domains were met successfully in an economic and manufacturable manner.

Development of MEMS products is currently hampered by the need for design aids, which can assist in integration of all domains of the design, see Senturia (1998), Wachutka (1999). The cross-disciplinary character requires a top-down approach to system design which, in turn, requires designers from many areas to work together in order to understand the effects of one sub-system on another. What is required is a design methodology based on concurrent design in all required domains. These design domains include the MEMS/MOEMS device, the analog sensing circuitry, the high-level system electronics, the application specific package, and manufacturing sensitivity analysis.

The ability of MEMS devices to be integrated with signal conditioning circuitry and batch fabrication offers an important advantage over their macroscopic counterparts. To ensure proper functioning of such an integrated system, one must perform system-level simulation. Such system-level modeling is extremely useful in determining operation characteristics and verifying performance before the device is actually manufactured. This can reduce the need for prototype fabrication and test iterations and significantly reduce cost and time-to-market.

Performing full 3-D physical simulation within each time step of a typical system simulator (such as SABER, MATLAB, or SPICE) is prohibitively time-consuming and numerically impractical. Hence, in order to simulate the appropriate system level dynamic behavior efficiently, a reduced-ordered model or "macro-model" of the MEMS subsystem must be obtained and employed in the system-level simulator. Thus, macro-model construction is a key part of a design methodology, see Romanowicz (1998).

As micro-systems become more complex and the need for models with large numbers of coupled degrees-of-freedom (DOFs) increases, the use of automated tools for generating macro-models becomes increasingly important. Although macro-modeling techniques have been reported by some re-

<sup>1</sup> Microcosm Technologies, Inc., 215 First St., Ste. 219, Cambridge, MA 02142 U.S.A, Email: bfr@memcad.com.

<sup>2</sup> Ford Microelectronics, Inc., Colorado Springs, CO, U.S.A.

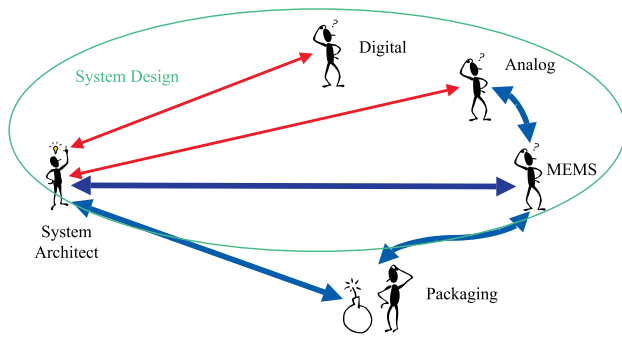


Figure 1 : Design groups involved in MEMS design

searchers, (see Fedder and Howe (1996), Swart, Bart, Zaman, Mariappan, Gilbert and Murphy (1998), Bart (1996), Lorenz and Neul (1998), Bart, Swart, Mariappan, Zaman and Gilbert (1998)), currently there is no systematic method for generating macro-models for MEMS devices in an automatic way.

Design tools to support this methodology must allow passing of models from one group to another to foster communication between them. These tools must also be usable by engineers who are not high level scientists with years of MEMS simulation experience.

In this paper we summarize some of the past three years work on developing methods and tools to enable the concurrent design of MEMS and MST systems. First we describe the concurrent design methodology itself, with particular attention to who does the designing and how different designers interact. We follow that with discussions of three research projects, which provide tools to enable the key arrows of Fig. 1. These are tools for automatic extraction of dynamic macro-models, tools for coupled package and device modeling in MEMS, and tools for the prediction of gas damping and spring effects on MEMS devices.

## 2 Concurrent design of MEMS

MEMS design involves several layers of design work, and potentially concurrent engineering among several groups. An “Actor” based view of such concurrent engineering is sketched in Fig. 1. A System Architect coordinates the design of a product, drawing on the knowledge and experience of design specialists in the digital and analog circuit, MEMS device, and packaging fields. Successful design of systems containing MEMS components requires a top-down approach to system design. This involves supporting the actors (design groups) in Fig. 1 with behavioral modeling and simulation at the level of the System Architect, and enabling the System Architect to specify subsystem functions in each area, by specifying behavioral models.

The use of electronic design automation (EDA) tools for the

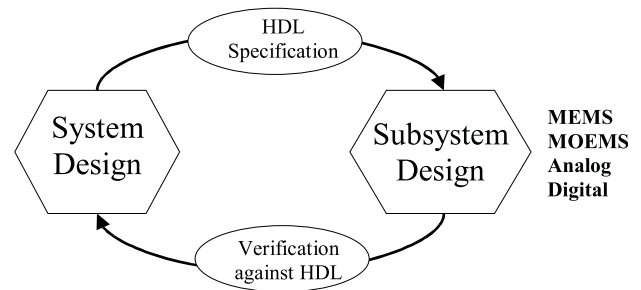


Figure 2 : Use of HDLs for specification and validation by system architect

system level simulation of MEMS is attractive, as complete systems may be simulated together with the physical transducers, analog and digital signal processing, compensation and control modules, and external environmental influences. The System Architect can investigate the effects of various design partitions, and trade off the complexity of the various subsystems, and verify if these options are compatible with the required system performance and functions.

### 2.1 Use of HDLs for design intent communication

Modern analog and mixed signal hardware description languages (HDLs) can advantageously be used to facilitate this communication between the design specialists. In our case, this corresponds to enabling the thick arrows in Fig. 1. The use of HDLs, as opposed to SPICE models, for system level simulation supports the use of energy-based physical models. This prevents the introduction of spurious energy sources, which can occur, for example, by using SPICE polynomial sources to model nonlinear elements. HDLs also provide a rich set of syntax, constructs, and modeling methods, see Senturia (1998). These are needed to describe the complex coupled physics present in transducers in an accurate and efficient manner. Signal flow modeling, a technique is often used for the analysis of systems containing feedback loops, is supported by HDLs. This is the approach used by tools such as the Simulink™(in Matlab™). The advantage of using a circuit simulator is the ability to seamlessly introduce models of electronics in the feedback loop.

HDLs also support various *levels of abstraction*, which may be introduced by the System architect as he refines the system from an initial set of components with simplified behavior, to more sophisticated models which contain detailed information about the performance of subsystems, as provided by the various actors.

The System Architect specifies the targeted functionality of each subsystem, as needed to fulfill the required system performance, using VHDL-AMS or a proprietary HDL such as Mast™, VerilogA™, SpectreHDL™, HDL-A™, etc. He can

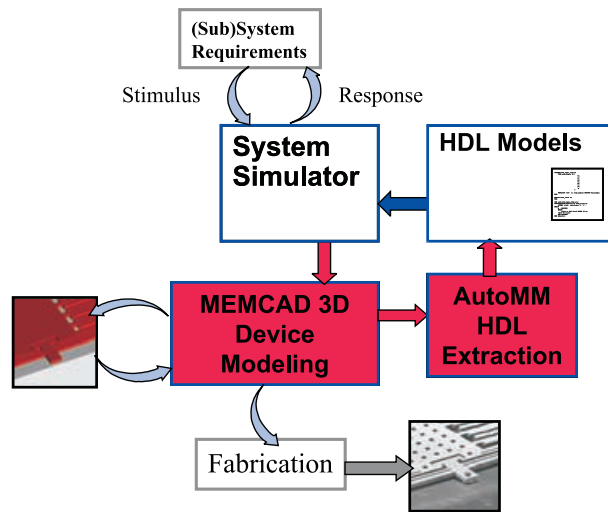


**Figure 3** : MEMS device design inside the system design loop

perform a system level simulation with these behavioral models to validate the system performance, and validate design partitioning that he has made. For example, it is possible to trade off complexity in the design of a physical transducer against the complexity in the signal processing subsystem. The System Architect then passes each of these behavioral models to the design specialists in each field. These behavioral models are in effect design specifications, which the subsystem designer must now meet. This design process is illustrated in Fig. 2.

Each of the design specialists may now work independently on his subsystem to insure that it meets the targeted functionality that is required of it. An example of such a design process, and the CAD tools that support it, is presented in Fig. 3. A MEMS inertial sensor subsystem designer receives a specification from the System Architect. After drafting a set of layouts corresponding to the process he wishes to use in manufacturing the device, he then performs an accurate 3D simulation to capture the physics, which are of importance in his design. He then automatically extracts parameters of importance in this design, to create a reduced order model in a HDL of his choice. This behavioral macro-model can now be simulated and compared to the abstract specification provided by the system architect, to verify if the device design provides the required functionality.

The above process is interactive. If any of the actors are unable to meet a targeted specification, they provide the System Architect with a behavioral model of their best design. The System Architect may then change the specification of another subsystem, in order to compensate for the actual performance of a subsystem. This design process is iterated upon until an optimal design is obtained. These decision criteria may include technical specifications such as performance, accuracy,

speed, size, power consumption, functionality, but can also include economic and marketing considerations such as cost, reliability, time to market, dimensions. Costly and time consuming prototyping steps are thus avoided.

This top-down approach to MEMS design does place considerable constraints on the CAD tools, as well as on the foundries and plants where the devices are to be manufactured. Without accurate knowledge of parameters such as material properties, residual stresses, manufacturing repeatability, operating conditions, packaging stress, etc. a CAD system can not operate in a predictable manner. In an analogous manner to electronic design automation (EDA), MEMS CAD requires the existence of foundry, process, and even run specific data to predict product performance with an acceptable accuracy. This implies the existence of systematic process characterization through test structures, and the calibration of the CAD tools using constitutive properties extracted from these test structures.

## 2.2 System design partitioning issues

As indicated in Fig. 1, MEMS devices are composed of multiple sub-systems, which are designed separately and must be integrated. This requires not only communication between the sub-system designers as previously discussed, but also an integrated view of how to partition the sub-systems for optimal cost and performance. Integrated or single chip MEMS are usually manufactured using a set of pre and post CMOS micromachining steps using fab compatible materials. An example of an integrated system is the Analog Devices automobile airbag accelerometer, see Spangler and Kemp (1995). Integrated devices are attractive because of their generally low unit cost in mass production. The integration of electronics close to sensors also helps noise performance.

Hybrid MST systems offer a greater choice of technologies and materials for the physical transducer, thus offering possible advantages in performance. They are however potentially more costly to package and assemble, and signal conditioning may be problematic as parasitic impedances are introduced between the sensor and front-end electronics. Ford Microelectronics uses a two-chip hybrid system for their airbag accelerometer, see MEMCAD 4 (1999).

Efficient communication between the actors in Fig. 1 is required for both a single chip approach, and for a hybrid multi-chip system solution. The interaction between the designers will be simpler in the second case, as they will not (necessarily) be sharing the same silicon die. The exchange of energy and information between subsystems on different chips will take place through the various interconnects (electrical, fluidic, optical, etc.) connecting the separate substrates. Here, the specifications provided by the System Architect will reflect the structural partitioning provided by the multi-chip approach. In both cases however, the CAD support tools supporting the design flow will be similar.

In both integrated or hybrid MEMS, electronics are used to

improve the sensor performance by linearization schemes, active feedback, thermal compensation, chopping to reduce  $1/f$  noise etc. Other system level electronics are often required such as sensor calibration, self-test, programmability and other application specific functions. Additionally design trade-offs are required such as the choice between integrating an on-chip pre-amp versus a complete A/D converter. The partitioning of these sub-systems can have a significant effect on the system performance. System level modeling is critical to optimizing this partitioning.

In inertial measurement systems it is possible to trade complexity between the mechanical and electronic subsystems. A cheap and nonlinear sensing element may be improved through linearization and feedback, but this implies additional IC real estate. For example, a closed-loop system may be used to remove all mechanical and geometric non-linearity's in an accelerometer by sensing the position of the seismic mass and applying a correction force equivalent to the acceleration, thereby immobilizing the mass at its point of rest. Care must be taken here to ensure that mechanical resonance frequencies are not excited by capacitive sensing means, which requires a mechanical-electronic co-design. This type of force-feedback design was used in initial accelerometer designs, see Spangler and Kemp (1995). When improved system modeling demonstrated the linearity of the mechanical part, the feedback was discarded in favor of a smaller, cheaper circuit, see Bart and Samuels (1996).

Another example occurs in resonant sensors such as MEMS gyroscopes. Here it is possible to trade off mechanical complexity in the form of the resonator Q versus the phase accuracy of the sensing electronics. The trade-off point can be very dependent on the specifics of the design (including the fabrication process constraints) and requires modeling to optimize. All of these design tradeoffs can be taken into account through efficient top-down behavioral model generation and bottom-up validation procedures. Examples of products whose design is supported in MEMCAD today include:

- Inertial Sensors
- Pressure Sensors
- Mirrors, Gratings, Optical Switches
- Electrical/RF Switches
- Thermal Actuators/Sensors
- Packaging Analysis
- Ink Jets
- uTAS and Lab-On-Chip Applications
- Flow Sensors
- Data Storage

In the following sections, we present research and simulation results of CAD tools we have developed to enable and support this design methodology. These sections correspond to

the thick arrows in Fig. 1. Sec. 3 describes a tool for automatic extraction of macro-models of electromechanical devices. A method for extracting compact models of MEMS packages, and linking them with device simulations is presented in Sec. 4. Finally, in Sec. 5, we present some results of characterization of squeezed film damping, often present in miniature structures, which can be applied to reduced order modeling of MEMS devices.

### 3 Extraction of macro-models

In this section, we describe a systematic method for modeling the class of electro-mechanical micro-systems that can be represented as multi-component, lumped, mass-spring-dashpot structures. Examples include accelerometers, gyros, and other structures that have rigid masses and compliant springs. In this lumped modeling assumption, the lumped spring effect originates from mechanical reaction forces and moments of the suspensions (or tethers) holding the proof-mass. Damping forces result from multiple energy loss mechanisms, but are dominated by gas viscosity. In addition, there are electrostatic forces and torques exerted on the dielectrically separated conductors in the system when voltages are applied. The accuracy of the developed method is verified by comparison of two plate-tether MEMS structures to results obtained from the developed models with those from full 3-D physics simulations. Good accuracy is demonstrated in both spatial-domain and frequency-domain dynamic behavior of the models.

#### 3.1 Overview

A semi-automatic and complete modeling procedure that automates the generation of component-level macro-models of MEMS devices has been developed, see Zaman, Bart, Rabinovich, Ghaddar, Tchertkov and Gilbert (1999). The user assembles the system-level model by connecting individual component-level macro-models together. For simplicity, the developed method assumes that while the tethers provide mechanical compliance, they are electrostatically inert and massless. It also assumed that the proof mass is electrostatically driven and moves as a rigid body. Devices that do not move as a rigid body, such as membrane devices cannot be accurately modeled with this technique.

The procedure begins by dividing the whole device into sub-components such as mechanical springs, electrostatic elements, dashpots, and proof-masses. These subcomponents are separately meshed and simulated over the desired ranges of operation. These full 3-D physics simulations are done in MEMCAD, see MEMCAD 4 (1999), using hybrid finite element and accelerated boundary element physics. The results of these simulations are fitted to multi-variable polynomials as functions of the desired degrees of freedom (DOFs). The macro-models for each subcomponent are then automatically generated in the behavioral modeling language of a system level simulator (SABER, SPICE, etc.). Finally, the component-

level macro-models are assembled into a system-level design to model the behavior of the whole system.

### 3.2 Theory

The modeling approach assumes coupling between three translational degrees of freedom (DOFs) and three rotational DOFs. While the translational DOFs are aligned with the axes of a general three-dimensional coordinate system, a rather complex notation is used to denote the rotational degrees. According to Euler, any rigid body rotation can be described as one effective rotation around an arbitrarily oriented rotational axis.

The effective rotation is defined by its three components  $\theta_x$ ,  $\theta_y$ , and  $\theta_z$  as follows:

$$|\theta| = \sqrt{\theta_x^2 + \theta_y^2 + \theta_z^2}$$

The unit rotation vector is defined as

$$a\hat{i} + b\hat{j} + c\hat{k} = (\theta_x\hat{i} + \theta_y\hat{j} + \theta_z\hat{k}) / |\theta|$$

Hence, the position vector is comprised of three translations and three rotations:

$$x = [xyz\theta_x\theta_y\theta_z]^T$$

The complete system model is expressed as a set of equations for each of these degrees of freedom. The complete system assumes equilibrium in total system energy. Equilibrium in the DOFs is achieved by balancing the total force and torque acting on the system. For a typical mass-spring-dashpot structure, the force-balance takes the following form:

$$f_{ext} = f_s + f_e + f_d + f_m \quad (1)$$

where  $f_{ext}$  is the force applied by external acceleration or other force sources (if any),  $f_s$  is the mechanical spring reaction force,  $f_e$  is the electrostatic force,  $f_d$  is the damping force, and  $f_m$  is the inertial force experienced by the proof mass. The torque-balance equation takes a form similar to Eq. 1. In the general case, Eq. 1 is a vector equation in six degrees of freedom,  $x$ , and all  $f_s$  are matrices. Each matrix element of  $f$  can be expanded in a Taylor series where we can choose the number of terms we care to retain. For example, a constant term in  $f_s$  represents a simple linear spring constant in a system where the degrees of freedom are uncoupled,  $f_s = k_s x$ . In a six DOF system,  $k_s$  can be represented by a polynomial hyper-surface coupled in six degrees of freedom. In the work described here we keep terms up to fourth order. The coefficients of these polynomial expressions are found from full 6-D simulations of different physical effects, described below.

### 3.3 Component level equations of motion

The equations of motion for the total structure are found by combining the mathematical model for each individual component. Following is a brief description of the system equations of a few representative MEMS components:

#### 3.3.1 Proof mass

A proof mass in a MEMS system is described by its mass, constant moments of inertia in its body-centered fixed coordinate system, and its center of mass. In a multi-DOF system, the coupling and interaction between the translational and rotational DOFs results in complex equations of motion for the proof-mass dynamics. A well-known part of this complex cross-coupling is the Coriolis effect. In order to be able to accurately predict the coupling between different DOFs and the dynamic motion of the proof-mass, one must retain the rotational coupling terms.

**Force Equations:** The forces along the linear DOFs are given by, see Shames (1997):

$$F = m(\dot{v} + \omega \times v) \quad (2)$$

where  $F$  is the force vector and  $m$  and  $v$  are respectively mass and linear velocities.

Hence, the force components are given by

$$m \begin{bmatrix} \ddot{x} \\ \ddot{y} \\ \ddot{z} \end{bmatrix} + m \begin{bmatrix} 0 & -\omega_z & \omega_y \\ \omega_z & 0 & -\omega_x \\ -\omega_y & \omega_x & 0 \end{bmatrix} \begin{bmatrix} \dot{x} \\ \dot{y} \\ \dot{z} \end{bmatrix} \quad (3)$$

**Moment Equations:** The moments around the center-of-mass coordinate axes are given by:

$$M = \dot{H} + \omega \times H \quad (4)$$

where  $M$  is the moment vector and  $m$ ,  $v$ ,  $H$ , and  $\omega$  are respectively mass, velocity vector, angular momentum vector, and angular velocity vector. The angular momentum  $H$  is computed from the moment of inertia matrix and the angular velocity vector:

$$\begin{bmatrix} H_x \\ H_y \\ H_z \end{bmatrix} = \begin{bmatrix} I_{xx} & -I_{xy} & -I_{xz} \\ -I_{yx} & I_{yy} & -I_{yz} \\ -I_{zx} & -I_{zy} & I_{zz} \end{bmatrix} \begin{bmatrix} \omega_x \\ \omega_y \\ \omega_z \end{bmatrix} \quad (5)$$

To avoid computation of varying moments of inertia of the proof-mass in the global coordinate system, these equations are computed in a frame of reference firmly attached at the body center of the proof-mass, thus making it subject to the rotations and translations that the mass experiences. The forces and moments so computed are then transformed to the global coordinate system in order to perform system-level simulation. The moment equations in the global coordinate system are found by

$$M_{XYZ} = TM_{xyz} \quad (6)$$

where  $T$  is the transformation matrix between the global ( $XYZ$ ) and *local* ( $xyz$ ) coordinate systems.

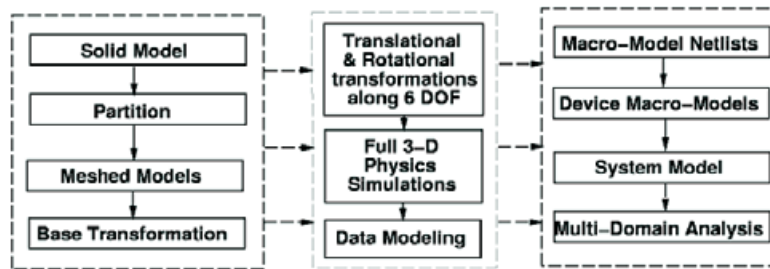


Figure 4 : Sequence of Operations

### 3.3.2 Tether

The forces and moments exerted by a mechanical tether are represented by:

$$f_s = k_s x$$

where  $k_s$  is a combination of different order matrices with coupling coefficients between different DOFs.

### 3.3.3 Electrostatic elements

Electrostatic forces are found by computing the spatial derivative of electrostatic energy:

$$f_e = \frac{1}{2} V^t \frac{d|C_{ij}|}{dx} V \quad (7)$$

Eq. 7 yields the electrostatic force as a function of one degree of freedom ( $x$ ). Generalizing this to  $n$  degrees of freedom, the derivative becomes the spatial derivative of the  $n$ -dimensional capacitance surface.

### 3.3.4 Damper

The forces and moments exerted by a damper are computed by the following equation:

$$f_d = k_d \dot{x}$$

where  $k_d$  is the damping coefficient matrix and  $\dot{x}$  is the spatial first-derivative of the DOF vector  $x$ .

### 3.4 Reusable components

Most practical inertial MEMS devices contain multiple tethers and one or more electrostatic structures (e.g., combs), which are connected to the proof mass at multiple positions and orientations. Since these components are typically identical, one would like to perform detailed 3-D analysis only once and use the resulting model at multiple locations in the system model.

In the developed modeling technique, the mechanical springs and electrostatic force elements are simulated as independent entities in their local coordinate system. This allows them to be used in any device model with the help of converters

that transform the degrees of freedom (translational and rotational), forces, and moments between these two systems. Another set of transformations are needed to transform the forces and torques applied by the spring at the location where it is connected to the center of mass of the proof mass. This allows the proof mass to be treated as a rigid body with its mass concentrated at its center of mass. These transformations include various types of Euler's and rotational transformations (and their inverse transformations) between coordinate systems.

### 3.5 Implementation

The modeling technique has been implemented in a tool named AutoMM (Auto Macro Modeler). The basic steps involve exploring the device operation space, modeling the data through multi-degree polynomial curve-fitting, and using the polynomial coefficients and other simulation data in dynamic equations. AutoMM consists of several sub-modules that are used to simulate the electrostatic, mechanical and inertial behavior of MEMS components in their operation space as a function of the DOFs.

AutoMM is built around the basic functionalities of the MEMCAD software tool suite, see MEMCAD 4 (1999). It directly uses the MEMCAD device creation and visualization methods and applies wrappers around the solver modules. AutoMM is constructed as a collection of functional sub-modules. This allows the flexible addition of components with different physical behaviors. It also allows the calculation of the behavioral data to be done in parallel, which reduces the over-all time of macro-model generation.

#### 3.5.1 Sequence of operations

Fig. 4 shows the sequence of operations that are carried out by the AutoMM module to generate macro-models. The procedure starts by creating the device solid model using the 'Mem-Builder' module of MEMCAD, see MEMCAD 4 (1999) from the device process information and the device layout. Then a finite-element mesh is created on the solid model. This meshed solid model is input to the AutoMM module which first carries out a global base transformation on the meshed structure according to the specifications provided by the designer. Examples of such transformations include changing separations of

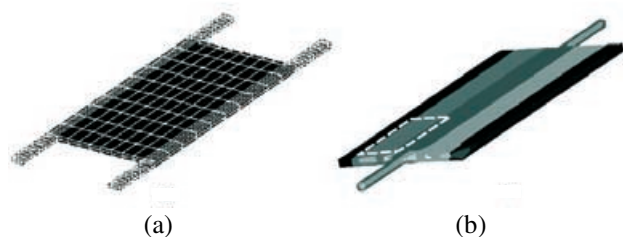


**Figure 5** : (a) Finite element mesh of example plate-tether structure, (b) Dominant mode-shape in Rotational-Y degree of freedom for example torsional mirror. (Dotted line shows approximate position and size of electrode underneath the plate).

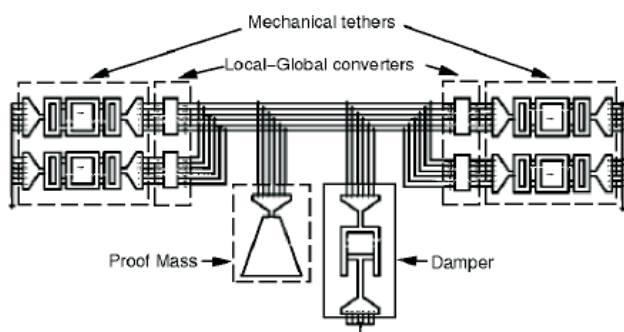


**Figure 6** : Schematic of the plate-tether structure model build from lumped elements (Through Variables: force, torque, current; Across Variables: position, angle, voltage).

structures, angular orientations, lengths, thicknesses, density, Poisson ratio, stress, and other geometrical and material properties of different subsets of device components. Note that this step can account for the effects of manufacturing variations in the final device macro-model.

The transformed models are then passed to the sub-modules that perform electrostatic, mechanical, and inertial simulations using multi-DOF boundary conditions. The simulation data are then fit to multi-degree polynomial equations (up to fourth order), which are functions of the degrees of freedom over which the device has been simulated. These polynomial fit coefficients are finally used in system equations to create the device macro-model. Although most of these steps are automated, user interactions and interventions have been allowed in a few cases to include the capability of monitoring the simulation process and specification of user-defined macro-model parameters.

### 3.6 Verification

In order to verify the accuracy of this modeling technique, we have examined several MEMS structures. Here we present results for two of them. The first one is a simple horizontal plate

structure with four parallel tethers at the four corners. Fig. 5(a) shows the mass-spring meshed structure.

Fig. 6 shows the equivalent system model implemented in the SABER simulation tool. The results of the lumped modeling technique are compared to the resonant frequency results of full 3-D physics simulation. Fig. 8 shows the frequency response from the model for all DOFs. Tab. 1 compares the modal frequencies found from the model and full 3-D physics simulation, which show good agreement.

**Table 1** : Comparison of modal frequencies obtained from AutoMM model and full 3-D physics simulation for plate-tether structure in Fig. 5(a).

Degrees of Freedom	AutoMM	Full 3D	%Error
Translational X	811.91K	825.23K	-1.61
Translational Y	4421.7K	4342.8K	+1.82
Translational Z	433.39K	431.06K	+0.54
Rotational X	920.52K	939.29K	-1.99
Rotational Y	716.11K	710.70K	+0.76
Rotational Z	3439.8K	3428.8K	+0.32

**Table 2** : Comparison of displacements and rotations in the dominant DOFs between full 3-D simulation and AutoMM results for two voltages (pull-in occurs at 219 volts). F3D, AM, and %E indicate full 3-D physics simulation results, AutoMM results, and percentage errors, respectively.

DOF	25 Volts			150 Volts		
	F3D	AM	%E	F3D	AM	%E
Tz (nm)	-1.60	-1.56	2.5	-65	-60	7.7
Rx ( $\mu$ rad)	2.526	2.46	1	102.5	89.6	12.6
Ry ( $\mu$ rad)	40.95	39.5	3.5	1700	1550	8.8

**Table 3** : Comparison of modal frequencies obtained from AutoMM model and full 3-D physics simulation for torsional mirror in Fig. 5(b).

Degrees of Freedom	AutoMM	Full 3D	%Error
Translational X	593.19K	583.53K	+1.66
Translational Y	3034.0K	3070.8K	-1.20
Translational Z	297.38K	304.82K	-2.44
Rotational X	672.54K	664.19K	+1.26
Rotational Y	169.02K	165.36K	+2.21
Rotational Z	1111.3K	1138.3K	-2.37

A torsional mirror with a ground electrode was also investigated. The ground electrode is under one of the corner of the plate and two tethers suspend the plate. A voltage applied between the plate and the electrode tilts the mirror asymmetrically towards the fixed electrode. Fig. 5(b) shows a dominant

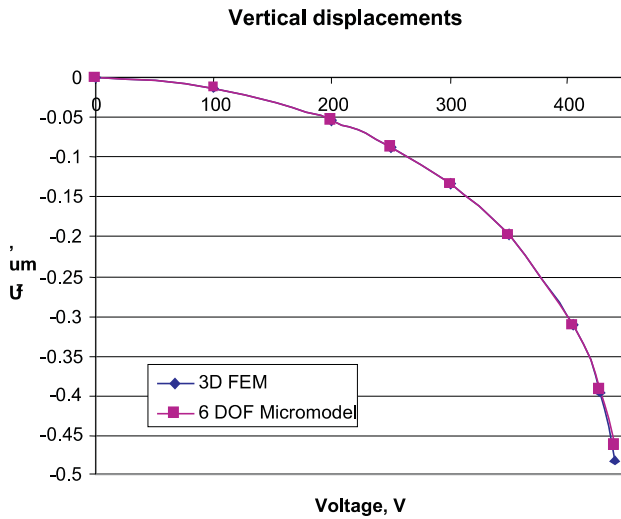


**Figure 7** : Comparison between full 3D CoSolve simulation, and 6DOF macro-model of plates structure in Fig. 5(a), for an electrostatic pull-in simulation.

mode-shape of the structure found from full 3-D physics simulation. Fig. 9 shows the equivalent system model. Fig. 10 shows the frequency response from the model and Tab. 3 compares the corresponding modal frequencies with those obtained from full 3-D physics simulation. Tab. 2 compares the changes in the dominant DOFs with applied voltage. The displacements and rotations show reasonable agreement to those found from the MEMCAD coupled, full 3-D electromechanical solver. The observed results also show that the error increases as the applied voltage gets close to the pull-in voltage.

**3.7 Conclusion**

A modeling procedure that automates the generation of macro-models of MEMS devices and shows good agreement to full 3-D physics simulation has been presented in this section. This tool corresponds to a software realization of the thick arrow between the *System Architect*, and the *MEMS designer* in Fig. 1. The implemented modeling technique is currently limited to the class of devices where the actuating and restoring forces are limited to electrostatic, mechanical (tensile and torsional), damping, and inertial types. Future developments will consider electrostatically active mechanical tethers with nonzero mass and macro-models for other physical forces, such as fluidic pressure, thermal stress, piezo-electric potential, etc.

**4 Coupled package-device modeling for MEMS**

All MEMS devices must be packaged in a manner appropriate to their applications. This packaging is often more specialized and expensive than the device itself. The package is the

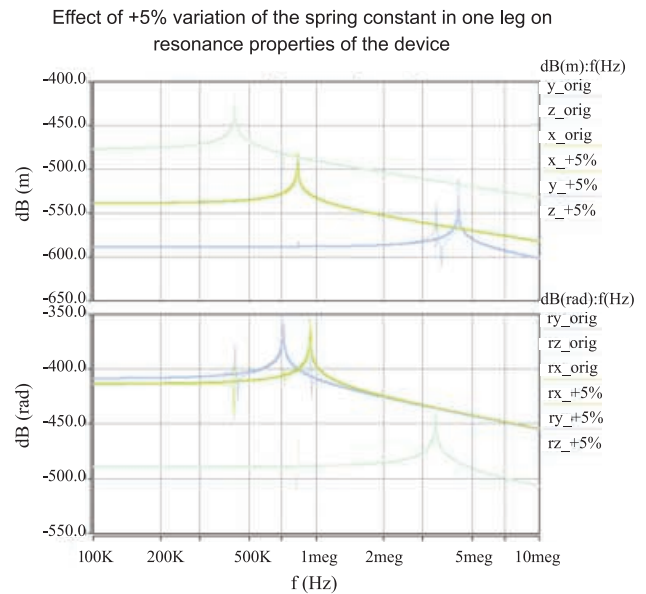


**Figure 8** : Frequency response in six degrees of freedom for the plate-tether structure in Fig. 5(a). The thick lines show the nominal response for the 3 translational and 3 rotational degrees of freedom. The thin lines are obtained with a 5% variation of the thickness of one tether, and show the mode coupling obtained when symmetry in the model is broken.

near environment of the device and hence has a direct effect on its thermal behavior, on mechanical effects, and on environmental compatibility and contamination. Package modeling in this context is the attempt to simulate these interacting effects so that the overall system behavior can be predicted and optimized.

MEMS/MOEMS packaging challenges are apparent when considering that there is a strong interaction of sensors and actuators with the environment. This can be seen in Electro-Magnetic interference, Optical, Thermal, and or mechanical transducers. Besides the direct influence of the “device” there can also be a significant influence of package stress/strain state on device geometry and functional specifications. The obtained stress/strain state is either due to the packaging process or some external influence such as a temperature change. Throughout this section we will use the word *device* to refer to a MEMS or MOEMS component. The word “package” refers to the housing in which the device is placed.

Besides the packaging challenges there are also modeling challenges. One problem, which almost always occurs in package/device modeling, is the tremendous difference in the size scale between device and package. Any combined Finite Element Method model with appropriate resolution will easily exceed the computational resources. Even when some solutions can be found the necessity of numerous simulations for

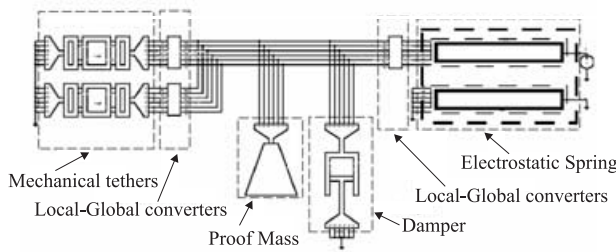


Figure 9 : Schematic of torsional mirror model.

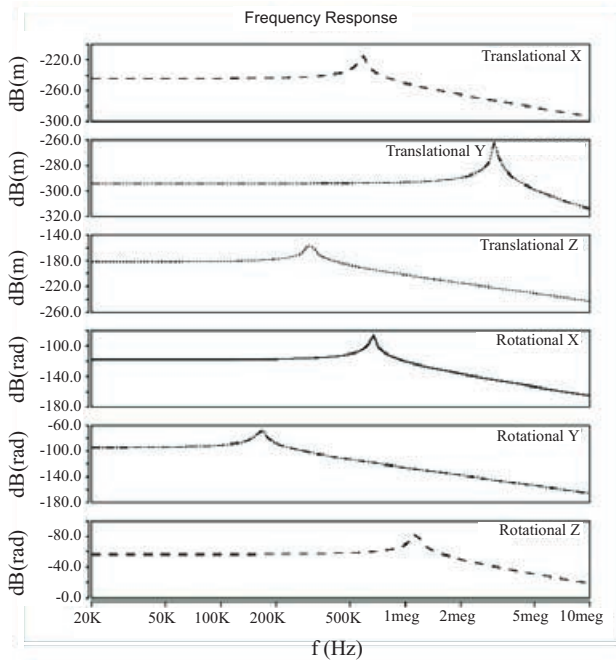


Figure 10 : Frequency response in six degrees of freedom for torsional mirror in Fig. 5(b).

exploration of the design space and various operation scenarios makes this “brute force” approach even less feasible.

To overcome this problem a modeling technique was developed which we will name the Compact Model Extraction (CME) technique. This approach allows for a separate analysis of the package and device. The package response to changes in the environment is modeled in the form of compact parametric models. These package-induced effects on a device can be simulated through appropriate boundary conditions based on compact model prediction. This methodology opens a possibility of creating the standardized libraries for package models that can be used in combination with new or existing device model.

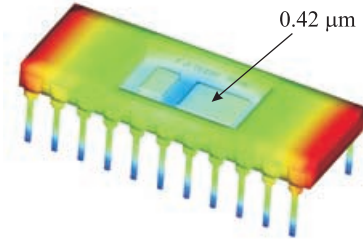


Figure 11 : A 3-D visualization of a thermo-mechanical package simulation done in the MEMCAD coupled package-device simulator. The color scale shows the displacement magnitude at  $125 \text{ }^\circ\text{C}$ . The probe shows the displacement magnitude at the center of the die.

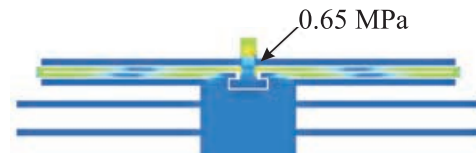


Figure 12 : A visualization of a thermomechanical stress simulation of a lateral accelerometer tether showing the temperature dependent stress caused by the coupling of the package in Fig. 1 to the device. The color scale and probe correspond to the stress magnitude at  $125 \text{ }^\circ\text{C}$ .

#### 4.1 Package-device modeling method

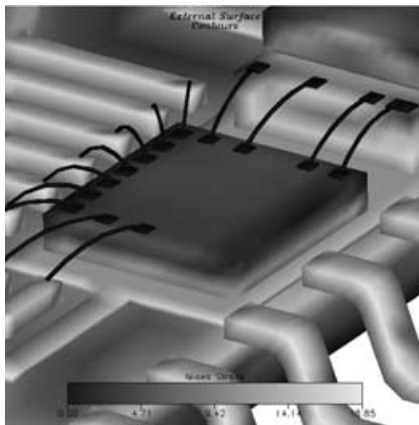
Since the MEMS device is small compared to the package, it is impractical to discretize a full package-device model at the density required to adequately model the device physics. We describe here a new capability to perform coupled package-device analysis based on the extraction of a compact representation of the package’s influences from FEA simulations of the package model only, see McNeil (1998), Bart and Gilbert (1998). The method begins with the construction and simulation of a 3-D package model. The user then chooses a surface region over which to fit a polynomial representation of the strain field. This region would normally be the die surface on which the MEMS device would be fabricated.

This compact model representation is then applied to a separate 3-D MEMS device model and simulated to predict coupled behavior. Fig. 11 shows the results of such a package simulation. Fig. 12 shows the stress induced by the package on a typical MEMS accelerometer device. Allowing the model to be parameterized over temperature extends the method above. Thus temperature induced package stress effects are correctly tracked during the MEMS device modeling.

The Compact Model Extraction approach uses two independent FEM models; one model for the package and one model

**Table 4** : Combinations of packages and devices investigated

	Package	Device
Set 1	Ford (plastic)	Analog XL-76
Set 2	Ford (Ceramic)	Motorola Accel.
Set 3	Motorola	Xerox mirror

**Figure 13** : Ford Plastic and Ceramic package. The figure shows a deformed view of some simulation results.**Figure 14** : Close up of plastic package model

for the device. To start the analysis, the package behavior under external influences is studied by passing the package FEM model through the solver. In most cases that would be a mechanical solver, solving for temperature change induced effects for example. The applied solver boundary conditions correspond to loads such as Temperature or heat flux to acceleration or external forces. Secondly the package boundary conditions are varied within a given range of the design space. An example with temperature sweeps will be presented later on. The resulting strain/stress fields of the package model under the different boundary conditions are stored and processed by the Packaging tool.

The next step is to capture this calculated package behavior in a compact description of the strained model; the Compact Model Extraction. To start the CME the Packaging tool calcu-

lates for a user-defined package/device interfacial planar surface (die surface) the displacement fields for all nodes within these surfaces for all values of changing external parameters. The next step is to run a curve-fitting program based on a Linear Least Squares SVD algorithm. A 4<sup>th</sup> order polynomial fit of the extracted displacement fields is performed as a function of spatial parameters since we are trying to describe the die surface (normalized local coordinates on a die surface). These polynomials are generated for each simulation point of the external influence parameter space. This set of polynomials constitutes the package parametric compact model for a given range of external parameters. A library of such compact models can also be generated.

Up until this step the FEM model of the sensor or actuator has not been used yet, which shows that these “package libraries” can be generated independently. In the following analysis one could think of the device being placed inside the package. This “attachment” of a device to a package can also be seen as applying the package as a boundary condition to the device. The simulation of the part now “feels” the package-induced environmental influences (temperature, etc.) as well as history dependent effects (such as built-in residual stresses). Before being able to run the device analysis a translation is needed from the Compact Model to the device boundary conditions. The Packaging tool projects the package displacement compact model onto the interfacial nodes of the device model based on user-defined placement of the device on the die surface and values of the corresponding external parameters. This means that the user is able to place the device anywhere in the package, provided that the location is on the surface that was used in the CME.

The user is also able to place the device anywhere in the external parameter space. This means that placing the device in the package is independent of the FEM mesh of the package, which was used to generate the original displacement field. It also means that if the temperature was varied and the package was simulated at a finite number of temperature points the device simulation can be done at any temperature between the maximum and minimum temperature.

This information on a device location and values of external parameters are used by the tool for of the displacement fields evaluation through curve-fitted polynomials for each “point” in external parameters range with consequent curve-fitting interpolation between the “points” at every node at the package/device interface. Resulting displacements represent the package-induced effects on a device and they are applied along with other appropriate boundary conditions for consecutive FEM analysis of the device model.

Note that because of interpolation between the “points” in external parameter space device can be simulated for any “point” within the range not only at the “points” at which actual simulation with the package model has been performed. In the CME method several assumptions are made in order to sim-

plify calculations. It is assumed that only the mechanical coupling from the package onto the device is important. In other words; the functioning of the device does not contribute to the stress/strain field of the package. There are however several techniques available to include the device induced effects in the analysis of the package. Boundary conditions during the package analysis can include the device effects such as heat or temperature sources.

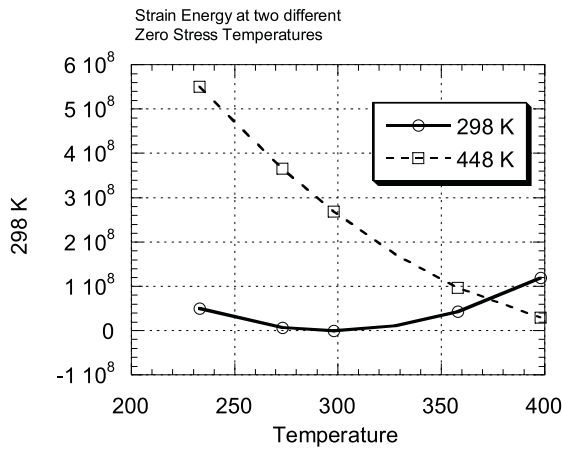


**Figure 15 :** Strain energy in the pyrex die on the ceramic package at different temperatures. The two graphs are for packages that have different zero stress temperatures.

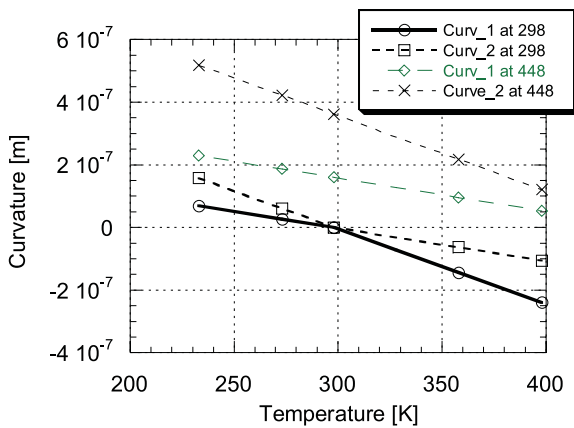


**Figure 16 :** Curvature in one direction of the pyrex die in the ceramic package. Same situation as in Graph 1.

**4.2 Simulation examples and results**

In this section the results of several Package/Device combinations are shown. Several packages were first ramped through a set of temperatures (from -40 to 125 °C). The combinations of package and device are shown in Tab. 4.

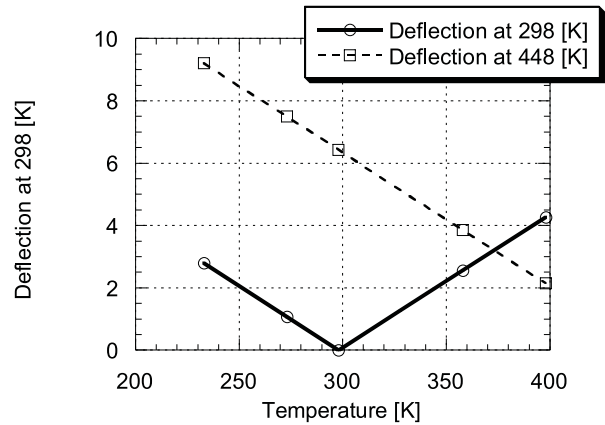


**Figure 17 :** Maximum deflection on the pyrex die top surface. In the “Deflection at 298 [K]” plot there is a sudden change in deflection. This is because the maximum deflection of the surface changes position from outer edge to middle point.



**Figure 18 :** Motorola package, shown in deformed view after simulation of the package at 200 °C

**4.2.1 Ford plastic package and ceramic package**

One of the package library components that we simulated using the Compact Model Extraction technique was a package developed by Ford. A solid model is shown in Fig. 13.

The same analysis was also run for a ceramic package, which is used later with a different device.

The Package is of a hybrid type. One die is a model with silicon material properties, which mimics the ASIC, that is located in the package. The second die is a Pyrex die, which represents the micromachined part. For the plastic package we removed the cap, the simulated package is shown in Fig. 14.

The package results themselves can be shown in several ways as well. First of all 3D pictures show the deformed state, Fig. 13. A better way of viewing quantitative results is by generating graphs. Fig. 15 for example shows the strain energy inside the pyrex die when the temperature is changed in the package. The two plots compare two packages where the only difference is the temperature at which the package is at zero stress. The next two figures show the curvature and maximum

deflection of the same pyrex die in the ceramic package. This is part of the data that is used to obtain the Compact Models.

4.2.2 Motorola plastic package

A third package that was used is a package based on a Motorola design. This is a MEMS specific package, which was also ramped over a temperature range. The package is shown in Fig. 18.

4.2.3 Analog devices XL76

A comb finger model of the XL76 accelerometer developed by analog devices was used in the device simulations. The accelerometer was passed through the Ford plastic package simulation. (Fig. 14).

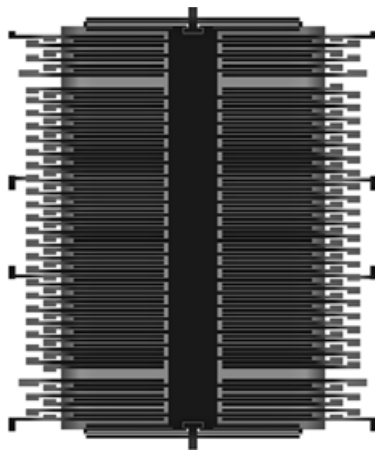


Figure 19 : Analog Devices XL76 solid model with stress color-coding.

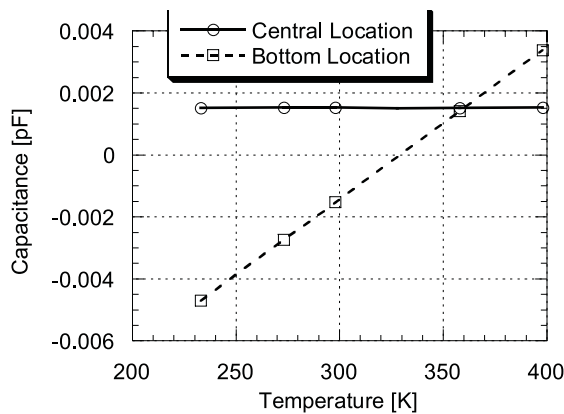


Figure 20 : Normalized relative capacitance change  $(C1-C2)/(C1+C2)$  between fixed fingers above (C1) and below (C2) movable finger

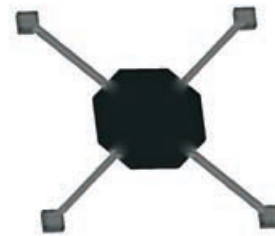


Figure 21 : Accelerometer based on the Motorola design. The four legs are attached to the package.

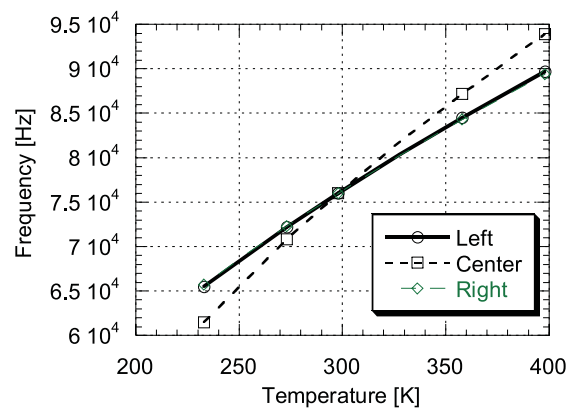


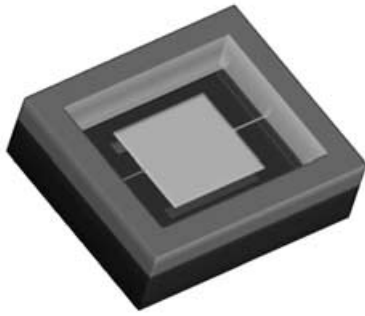
Figure 22 : Frequency of the Motorola accelerometer as a function of package temperature. The plot also shows a misalignment analysis. The “Left” and “Right” plot are exactly at the same location.

Fig. 20 shows the normalized relative capacitance change  $(C1-C2)/(C1+C2)$  between fixed fingers above (C1) and below (C2) movable finger. The comb accelerometer was put in the Ford plastic package and ramped through the same temperatures in this case.

4.2.4 Motorola accelerometer

With the accelerometer shown in Fig. 21 we did a modal analysis under the assumption that the device was packaged in the Ford ceramic package. The actual device also has capacitance detection electrodes under and over the accelerometer. Here we were interested in how the package influences the base modal frequencies.

Fig. 22 shows a result of placing the Motorola accelerometer from Fig. 21 in the Ford ceramic package. A modal analysis was done after the mechanical simulations. The results show a frequency change as a result of the package strains. There are two extra plots in the graph, which are exactly on top of each other. These are the result of miss-aligning the device with the



**Figure 23** : A Mirror suspended by two narrow tethers developed by Xerox.

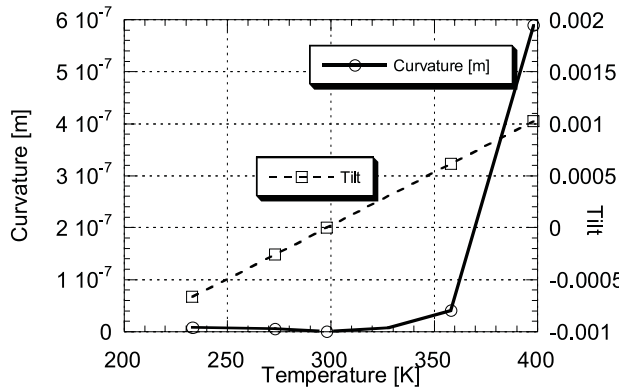


**Figure 24** : Curvature and Tilt of the Xerox mirror placed in the Motorola package.

package, a feature of the Memcad software.

4.2.5 Xerox mirror

As a last device a mirror developed by Xerox was passed through the Motorola MEMS device package shown in Fig. 18. The results are displayed as curvature and tilt in one direction. The results in Memcad are actually the curvature and tilt in 2D.

4.3 Experimental verification

In order to confirm the usefulness of this approach, we compare the results of experimental measurements to package stress predictions. The experimental characterization of packages involves the measurement of strain or displacement fields from which stress can be inferred, see Sweet (1993). Here we use off-the-shelf metal-film strain gages to measure the displacement field. To obtain accurate simulation results we wish to have a full mapping of the package strain onto the strain gauge. This is accomplished by treating the strain gauge as the

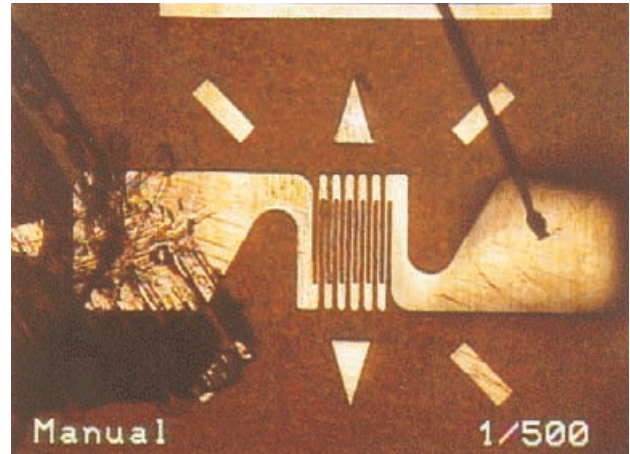


**Figure 25** : An optical micrograph of one of the metal foil strain gauges used for experimental calibration of the package model.

“device” in our package modeling method. This requires the addition of a simulation engine that allows the computation of the resistance change due to applied stress on the metal foil material. We report here experimental characterization performed for a Pyrex die (to represent a MEMS substrate) in a ceramic package. The die strain is measured over temperature and compared to the simulation results. Fig. 25 shows an off-the-shelf, metal-film strain gauge used for these measurements. Fig. 26 shows results for a coupled simulation of this strain gauge as affected by temperature induced package stresses. The simulation tool can directly calculate the change in resistance caused by these strains.

4.4 Advanced analysis

The simulation examples described so far are examples of obvious applications of the described software. In summary they are a direct mechanical analysis of package-induced effects on MEMS/MOEMS devices. As described in the introduction, meshing the package and device in one FEM model could have used any finite element analysis tool. The previous examples of packages and devices already used to additional option of pre-calculating the package and placing it in a library; by just pointing to the specific library in the device simulation the package is applied as a boundary condition without user intervention.

We have implemented the package/device analysis tool inside Memcad, which opens up the possibility of answering design questions for the package/device combination. Some design questions can be:

1. Which package is best for this device? If the device can be implemented in several packages, the device behavior can be compared if connected to these packages.

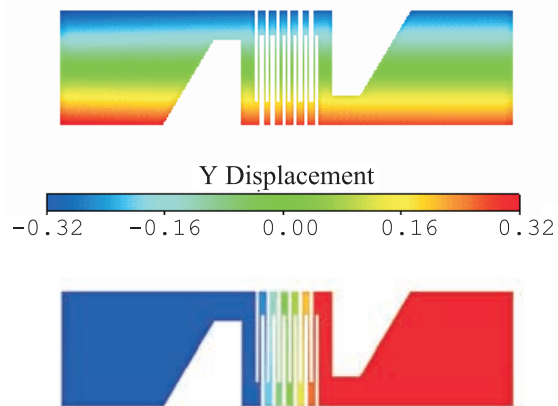


**Figure 26 :** These figures show 3-D FEM simulation results of the metal film strain gauge. In the upper figure, the color scale shows the displacement along the sensitive axis of the resistor element (vertical direction). The lower figure shows the potential distribution in the metal foil.

- Does the device still work within the set tolerances if it is misaligned with the package or even rotated? In the simulation manager of this software the device can be placed anywhere in the package. The default location is always the center of the attached surfaces.

#### 4.5 Limitations

Current implementation of the tool implicitly assumes that die surface is planar simply connected region. Moreover it is assumed that deformed surface of the die can be approximated by 4<sup>th</sup> order polynomials accurately though this limitation is not critical for the implementation. Another important underlying assumption of the CME method is an assumption that the device behavior does not influence the package. This assumption is valid for a wide variety of materials and dimensions combinations since devices tend to be much smaller than a die surface and device materials are not much stiffer than die materials in general. However for relatively stiff devices with a ratio of Young's modulus of device to package more than 10 and a ratio of device height to length more than 0.003 the difference between the actual strains and strains calculated for simplified case ignoring the influence of the device on package can be as high as 10%, see Alexandrov et al. To remove this limitation in a future a fully coupled package/device modeling scheme can be implemented. Coupling can be done on a level of compact models also. In the close coupling loop a compact model of reaction forces extracted from interfacial nodes in device simulation can be send back to package simulation in a form of reaction force type boundary conditions on relevant interfacial nodes in a package model. Several relaxation iterations between package and device simulations with cou-

pling through displacements (package to device) and reaction forces (device to package) boundary conditions can theoretically lead to a solution with mutual package/device interaction effects accounted for. This will be presented after it has been tested thoroughly.

#### 4.6 Conclusion

The effect of the packaging on a MEMS device's behavior cannot be ignored. In this section, we have demonstrated a methodology that creates a parameterized package macro-model and then applies this macro-model to the MEMS device to obtain coupled simulation results. This methodology is confirmed with package measurements instrumented with metal-film strain gauges. The CAD and associated methodology correspond to the thick arrows between the *Packaging* and *MEMS designers*, and between the *System Architect* and *Packaging Designer* in Fig. 1.

#### 5 Gas damping and sprint effects on MEMS devices with multiple perforations and multiple gaps

In this section, we describe research on a new method and tool for gas damping and spring prediction. The tool works on any arbitrarily shaped plate structure and allows analysis of such structures with multiple gaps and complex perforation (etch holes) patterns. It is accurate over a wide frequency range including both gas damping and spring dominated devices, and includes corrections for high Knudsen number effects. The section has three subsections: Sec. 5.2 a discussion of the models and method involved, Sec. 5.3 a discussion of the results of simulations, and finally Sec. 5.4 validation of the approach with experimental measurements. The experiments are from three different applications: a micro-relay (300KHz) from IMT, an accelerometer (1KHz) from Motorola SP, and an optical modulator (2MHz) from Lucent Technologies. The last two are examples of complex perforated structures.

##### 5.1 Motivation

A large class of MEMS devices must operate at significant gas pressures. To understand the dynamic behavior of these devices the effects of the gas surrounding the movable component can be critical. To accurately model devices such as accelerometers, switches, micromirrors, and resonant sensors requires an understanding of gas damping and spring effects. Most work in damping traces its lineage back to analytic modeling of the *Reynolds* equation by Blech (1983) for simple rectangular and circular plates. In recent years many groups have extended that work to make damping predictions more accurate or useful for more complex geometries. Approaches that have been reported are numerical solutions of the *Reynolds* equation, see Mehner, Kurth, Billep, Kauffman, Kehr and Dötzel (1998), or the incompressible *Navier-Stokes* (NS) equations, see Veijola, Kuisma and Lahdenperä (1997). Also, much

work has gone into correcting the *Reynolds* or incompressible NS equations for the effects of high Knudsen numbers, see Veijola, Kuisma and Lahdenperä (1997), Fukui and Kaneko (1998). Key difficulties with respect to these approaches are that the *Reynolds* formulation is not accurate for complex geometries such as perforated structures and the incompressible NS approach is unacceptable for realistic problems as it does not provide gas spring predictions due to its neglect of compressibility.

## 5.2 Models and methods

We are interested in the broad problem of the influence of the surrounding gas on a plate, membrane, or beam suspended next to one or more walls. In general if the plate moves with a small signal oscillation of frequency  $f$  perpendicular to the plate surface, the gas in the gap will exert a force back on the plate that has components in phase and out of phase with the velocity of the plate. The component in phase with the velocity is the gas damping force and that out of phase to it is the gas spring force. In order to make a complete model of the small signal behavior of the plate (such as would be appropriate for a sensor) one needs to accurately predict the damping and spring terms. Both terms are frequency dependent, and in principle, may be deduced from appropriate models of the physics of fluids in the regions near the plate. Both terms are pressure dependent and also dependent on the Knudsen number, see Veijola, Kuisma and Lahdenperä (1997), for each plate-gap system in the device.

The full NS equations would in general describe the viscous, pressure and inertial effects of the gas in the gap (will not be discussed here). In certain cases where the inertial effects are very small ( $Re \sim 1$ ) and the pressure drop across the gap is negligible ( $\delta p / \delta h \sim 0$ ), the NS equations simplify to the Isothermal *Reynolds* equations. Fluid film lubrication and squeeze damping fall into this class of problems where the thickness of the film or gap is significantly smaller than other relevant dimensions in the problems. Further if we make the assumption that the structure is only subject to small amplitude displacements and pressure changes the Isothermal *Reynolds* equation may be linearized to diffusion like PDE, See Yang, Gretillat and Senturia (1997).

A brief discussion of the validity of the continuum assumption pertaining to both sets of equations is necessary. The flow approximation (continuum, no slip) is valid up to Knudsen numbers of  $10^{-2}$ . Above this value the flow enters a transition regime between continuous and free molecular flow and the equations are still valid with a relaxation of the slip condition. In most MEMS applications where squeeze effects are significant, it is seen that the range of Knudsen numbers can be quite large. Veijola, Kuisma and Lahdenperä (1997) and Mehner, Kurth, Billep, Kauffman, Kehr and Dötzel (1998), have demonstrated that in these situations the introduction of an effective viscosity, see Fukui and Kaneko (1998), and Mit-

sui (1993), dependent on the Knudsen number is valid.

$$\frac{\mu}{\mu_{eff}} = 1 + 9.638 \left( \frac{p_0 \lambda}{pL} \right)^{1.159} \quad (8)$$

The approach then is to construct a hybrid tool that makes use of a solution to the Reynolds equation in some regions (at least one for each gap) and uses a solution to either the compressible or incompressible Navier-Stokes equation in critical domains of each structure. This hybrid, integrated approach is called **Navier-Stokes-Reynolds** or **NSR**.

The first step for a given device would be to mesh the moving parts of the structure and all relevant gaps. An example of such a mesh is shown in Fig. 27. The *critical* domains are those near all edges and perforations in the structure. In these regions appropriate flow resistance models describe the flow of gas through the hole or out the edge. These resistance models have been previously extracted by solving the full NS equations for a range of hole sizes and gaps. The resulting flow resistance model can be expressed functionally by  $f = f(r, h)$ , where  $r$  is the radius of the hole and  $h$  is the adjacent gap. A similar extraction technique would be required for different perforation geometries (with appropriately different parameters). The solver then ensures that at the edge of the hole, the appropriate flow resistance is matched with the *Reynolds* equation solution through a *Neumann* type condition  $dp/dz = pf(r, h)$ .

We include adjusting all regions automatically for high Knudsen number effects (using (8)) and also take into account mode shape effects for those systems whose displacement is a modal deformation (as suggested in Yang, Gretillat and Senturia (1997), for beams and membranes). The mode shape effect is accounted for computationally by adding displacement source terms at each element face at the interface of the gap and mass. In the case of a rigid plate motion all these sources are identically equal. However, when the structure's flexibility (modal displacement) is considered, each of these sources is proportional to the modal displacement at the surface.

The NSR approach thus has near the computational speed of numerical (Finite Element) Reynolds methods on large problems with considerably greater accuracy for both gas damping and gas spring terms.

## 5.3 Simulation results

The approach has been thoroughly verified on test cases involving simple geometries where analytical models are readily available, i.e. rectangular and circular plates. The NSR predictions are seen to be in very good agreement with analytical solutions for such cases, see Blech (1993).

As described, a 3D model of the plate and all gaps is constructed including edge and perforation regions, which are declared on this mesh so that the domains for NSR can be established. The general output of the solver is shown in Fig. 28, which shows both the gas-spring and gas-damping coefficient

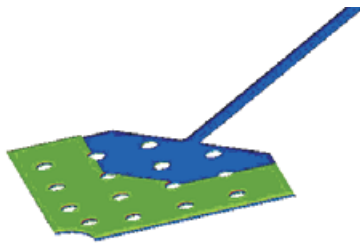


**Figure 27** : An example mesh (model), for the damping model of the Motorola accelerometer. Note, the exposed (infinite gap) surface.

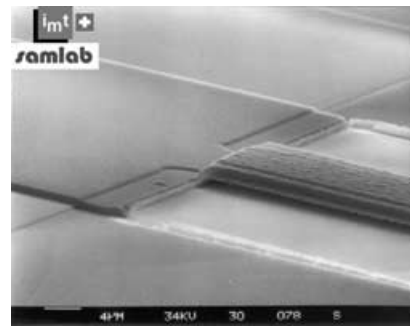


**Figure 29** : An SEM of microrelay from IMT.

vs. frequency for the Lucent problem (optical micrograph Fig. 29) discussed later.

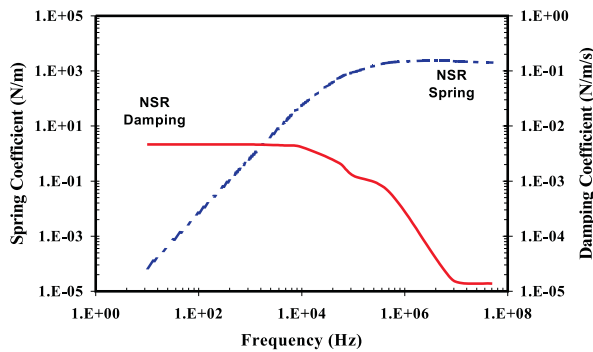


**Figure 28** : Typical output of Damping module NSR predictions of gas Damping and Spring vs. frequency for the Lucent sample 2 at P=0.5atm. (L2-P0.5-Ne).

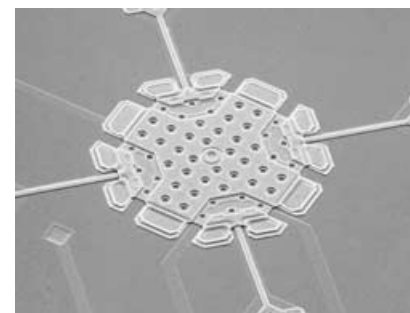


**Figure 30** : An SEM of the Motorola Accelerometer Device.

### 5.4 Experimental validation

Currently we have three experimental data sets for validation of the methods and models. The first is the IMT microrelay, see Gretillat (1997), Fig. 29 below, which is essentially a beam like structure. We include it to verify that NSR does not drift from the best Reynolds based techniques in the cases in which they are adequate, see Veijola, Kuisma and Lahdenperä (1997), and Gretillat (1997). The second is a low frequency accelerometer from Motorola SP, see Dao and Hammond (1998), shown in Fig. 30. The third is a pair of differently perforated circular membranes from *Lucent Technologies*, see Greywall, Busch and Bishop (1998), for an optical modulator application (one is shown in Fig. 30).

The latter two cases are devices with complex perforation patterns and structural geometry in which the Reynolds solution does not agree well with experiment and the incompressible NS would be computationally impractical. Tab. 5

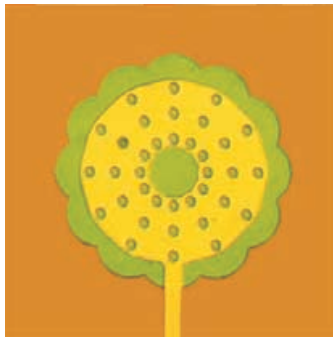
shows the comparison between the Reynolds equation, NSR and experiment for the damping coefficients for Motorola and Lucent. The NSR prediction is within experimental bounds for both data sets and shows significant improvement over the Reynolds solution.

Fig. 32 is a scatter plot in gas-spring vs. gas-damping showing all data and simulations for IMT (1 beam, 2 pressures), Motorola (one experiment), and Lucent (2 designs at 2 pressures each). The entire data set spans almost 5-7 orders of magnitude in each variable. In each case the experimental results have been shown (with appropriate error bars). Over this wide range, the NSR predictions show very good agreement.

Fig. 33 is a similar plot for the damping coefficient vs. fre-

**Table 5** : Comparison of Reynolds, NSR and Experiment for the Lucent and Motorola Problems (Damping has been normalized for comparison)

	L1-P0.5-Ne	M-P0.96-A
Expt	1.00	1.00
NSR	0.76	1.02
Reynolds	0.26	0.71



**Figure 31** : An optical micrograph of a high frequency optical modulator. (diam. of 150  $\mu\text{m}$ ) (courtesy Lucent Tech., see Greywall, Bush and Bishop (1998)).

quency showing that these experiments test the NSR technique over a wide frequency range from 1KHz to 2MHz.

**5.5 Conclusion**

In conclusion, we have detailed a new tool to solving the complicated problem of gas damping in MEMS devices.

The approach was then used to predict the behavior of three different devices over a wide range of operational regimes. The results are shown to be in good agreement with those observed in experiment. Further the accuracy and computational economy of using such an approach over a full NS simulation are of significant benefit to MEMS/MST designers of such devices. The NSR approach has been included in the damping module now available in MEMCAD 4.5.

**6 Summary**

Development of micro-electro-mechanical systems (MEMS) products is currently hampered by the need for design aids, which can assist in integration of all domains of the design. The cross-disciplinary character of microsystems requires a top-down approach to system design which, in turn, requires designers from many areas to work together in order to understand the effects of one sub-system on another.

In this paper we have summarize some of the past three years work on developing methods and tools to enable the concurrent design of MEMS and MST systems. First we described the concurrent design methodology itself, with particular attention to who does the designing and how different designers interact. We followed that with discussions of three research projects, which now provide tools to enable the key arrows of Fig. 1. These are tools for automatic extraction of dynamic macro-models, tools for coupled package and device modeling in MEMS, and tools for the prediction of gas damping and spring effects on MEMS devices.

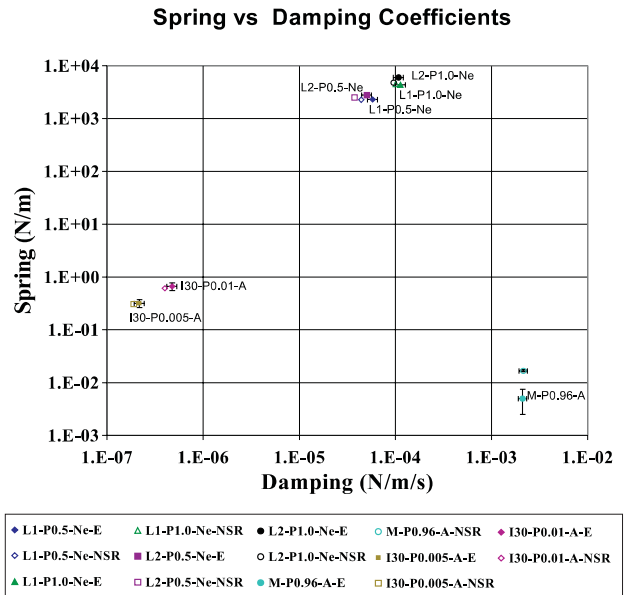


**Figure 32** : Scatter plot of Spring versus Damping coefficients for the 3 different devices. Note: L1-P0.5-Ne: Lucent Sample 1 at 0.5 Atm. Ne; L1-P1.0-Ne: Lucent Sample 1@ 1.0 Atm. Ne; L2-P0.5-Ne: Lucent Sample 2@ 0.5 Atm. Ne; L2-P1.0-Ne: Lucent Sample 2@ 1.0 Atm. Ne.

**Acknowledgement:** The authors acknowledge the support of the DARPA CiMEMS Program (Contract No. F30602-96-2-0290). The support of Jonathan Hammond (Motorola SP) and Dennis Greywall (Lucent Technologies) through many discussions is greatly appreciated.

**References**

**Alexandrov, V.** (1983): Assessment of error introduced by a strain gage in tensometry of low module materials. *Mechanics of Solids*, vol. 20.

**Andrews, M.; Harris, I.; Turner, G.** (1993): *A Comparison of Squeeze-Film theory with measurements on a microstructure*, volume 36.

**Bart, S. F.** (1996): CAD for integrated surface micromachined sensors: Present and future. In *the Proceedings of the Fifth ACM/SIGDA Physical Design Workshop*, pp. 72–75, Reston, VA.

**Bart, S. F.; Gilbert, J. R.** (1998): Integrating packaging into the MEMS sensor design process. In *Proc. of Sensor Expo*, pp. 469–472, Chicago.

**Bart, S. F.; R., S. N.; M., M.; Zaman, M. H.; Gilbert, J. R.** (1998): An environment for MEMS design and verification. In *Proceedings of 1998 International Conference on Modeling*

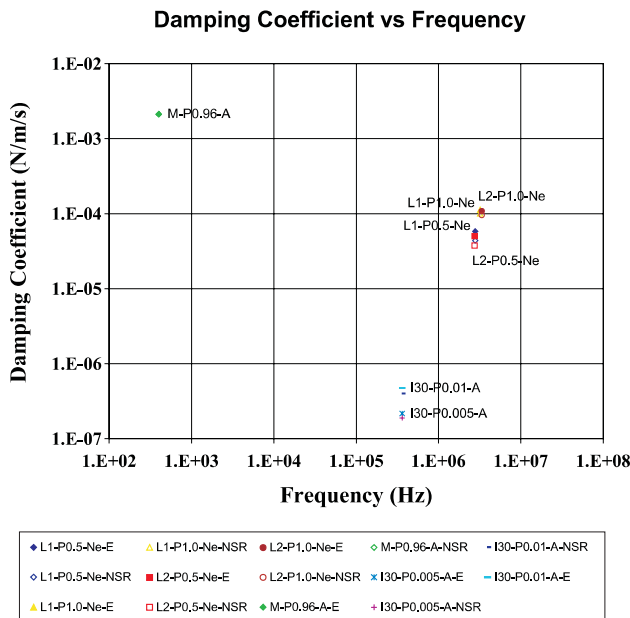


**Figure 33** : Scatter Plot of Damping Coefficient versus Frequency. Note: M-P0.96-A: Motorola Sample @ 0.96 Atm. (730T) Air; I30-P0.005-A: IMT Beam  $L=300 \mu\text{m}$  @ 0.005 Atm. Air; I30-P0.01-A: IMT Beam  $L=300 \mu\text{m}$  @ 0.01 Atm. Air In each case, the label on the graph is adjacent to both points -E & -NSR where E-Experiment; NSR-Navier-Stokes-Reynolds.

and Simulation of Microsystems, Semiconductors, Sensors and Actuators (MSM'98), pp. 386–391, Santa Clara, CA.

**Bart, S. F.; Samuels, H. R.** (1996): Design techniques for minimizing manufacturing variations in surface micromachined accelerometers. In *Microelectro-mechanical Systems, ASME, DSC*, volume 59, pp. 427–433.

**Blech, J. J.** (1983): On isothermal squeeze films. *Journal of Lubrication Technology*, vol. 105, pp. 615–620.

**Dao, P.; Hammond, J.** (1998): *Motorola Sensor Products*. Private Communication, Phoenix, TX.

**Fedder, G. K.; Howe, R. T.** (1996): Multimode digital control of a suspended polysilicon microstructure. *Journal of Microelectromechanical Systems*, pp. 283–297.

**Fukui, S.; Kaneko, R.** (1998): Analysis of ultra-thin gas film lubrication based on linearized boltzman equation: First report - derivation of a generalized lubrication equation including thermal creep flow. *J. Tribol. Trans. ASME*, vol. 110, pp. 253–262.

**Gretillat, M.-A.** (1997): *Electrostatic Polysilicon Microrelays*. Ph.D. Thesis, IMT, U. of Neuchtel, Switzerland.

**Greywall, D. S.; Busch, P.; Bishop, D.** (1998): *Phenomenological Model for Gas Damping of Micromechanical Structures*. Private Communication, Lucent Technologies, NJ.

**Lorenz, G.; Neul, R.** (1998): Network-type modeling of micromachined sensor systems. In *Proceedings of 1998 International Conference on Modeling and Simulation of Microsystems, Semiconductors, Sensors and Actuators (MSM'98)*, pp. 233–238, Santa Clara, CA.

**Manual, M.** (1999): Microcosm Technologies, Inc., 5511 Capital Center Dr., Raleigh, NC.

**McNeil, A. C.** (1998): A parametric method for linking MEMS package and device models. In *Proceedings of the Solid-State Sensors and Actuators Workshop*, pp. 166–169, Hilton Head Is. SC.

**Mehner, J.; Kurth, S.; Billep, D.; Kauffman, C.; Kehr, K.; Dötzel, W.** (1998): Simulation of gas damping in microstructures with nontrivial geometries. In *Proceedings IEEE MEMS 98*, pp. 172–177, Heidelberg, DE.

**Mitsui, Y.** (1993): *Modified Reynolds equation for Ultra-Thin film gas lubrication using 1.5 order slip flow model and considering surface accommodation coefficient*, volume 115.

**Neul, R.; Becker, U., L.; G., Schwarz, P.; Hasse, J.; Wünsche, S.** (1998): A modeling approach to include mechanical microsystem componets into the system simulation. In *DATE98 - Design, Automation and Test in Europe, vol. 1*, pp. 510–517.

**Romanowicz, B. F.** (1998): Methodology for the modeling and simulation of microsystems. In Senturia, S. D.(Ed): *Microsystems*. Kluwer Academic Publishers.

**Romanowicz, B. F.; Ansel, Y.; Laudon, M.; Amacker, C.; Renaud, P.; Vachoux, A.; Schrpfer, G.** (1997): VHDL 1076.1 modeling examples for microsystem simulation. In *Current Issues in Electronic Modeling, Issue No. 10*. Kluwer Academic Publishers.

**Senturia, S. D.** (1998): CAD challenges for microsensors, microactuators and microsystems. *Proc. IEEE*, vol. 86, pp. 1611–1626.

**Shames, I. H.** (1997): *Engineering Mechanics. Statics and Dynamics*. New Jersey.

**Sherman, S.** (1992): A low cost monolithic accelerometer. In *Proc. IEEE 1992 Int. Elec. Dev. Meeting*, pp. 19.1.1–19.1.4, San Francisco, CA.

**Spangler, L.; Kemp, C. J.** (1995): ISAAC - integrated silicon automotive accelerometer. In *Proc. of the 8th International Conf. of Solid-State Sensors and Actuators*, pp. 585–588.

**Swart, N. R.; Bart, S. F.; Zaman, M. H.; Mariappan, M.; Gilbert, J. R.; Murphy, D.** (1998): AutoMM: Automatic generation of dynamic macromodels for MEMS devices. In *Proc. 11th IEEE Intl. Workshop on Micro Electromechanical Systems (MEMS'98)*, pp. 178–183, Heidelberg, Germany.

**Sweet, J. N.** (1993): Die stress measurement using piezoresistive stress sensors. In Lau, J.(Ed): *Thermal Stress and Strain in Microelectronics Packaging*, pp. 221–271, van Norstrand Reinhold, New York.

**Veijola, T.; Kuisma, H.; Lahdenperä, J.** (1997): Model for gas film damping in a silicon accelerometer. In *Proceedings Transducers 97 Vol. II*, pp. 1097–1100, Chicago, IL.

**Wachutka, G.** (1999): The art of modeling coupled-field effects in microdevices and microsystems. In *Technical proceedings of the 1999 International Conference on Modeling and Simulation of Microsystems, MSM 99*, pp. 14–19, San Juan, Puerto Rico, U.S.A.

**Y.-J. Yang, Y.-J.; Gretillat, M.-A.; Senturia, S.** (1997): Effects of air damping on the dynamics of nonuniform deformations of microstructures. In *Proceedings Transducers 97 Vol. II*, pp. 1093–1096, Chicago, IL.

**Zaman, M. H.; F., B. S.; Rabinovich, V. L.; Ghaddar, C. K.; Tchertkov, I.; Gilbert, J. R.** (1999): A technique for extraction of macro-models in system level simulation of inertial electro-mechanical micro-systems. In *Technical Proceedings of 1999 International Conference on Modeling and Simulation of Microsystems, MSM 99*, pp. 163–167, San Juan, Puerto Rico.

